Oxygen reduction reaction monitored during corrosion by means of pumped-micropipette delivery/substrate collection (Pumped-MD/SC) mode of scanning electrochemical microscopy

Abdelilah Asserghine, Sophie Juillard, Julie Ducrot, Vincent Vivier, Carlos Sánchez-Sánchez

Oxygen reduction reaction monitored during corrosion by means of pumped-micropipette delivery/substrate collection (Pumped-MD/SC) mode of Scanning Electrochemical Microscopy

Abdelilah Asserghine[& 1], Sophie Juillard[1], Julie Ducrot[2], Vincent Vivier* [1,3], Carlos. M. Sánchez-Sánchez** [1]

[1]*Sorbonne Université, CNRS, Laboratoire Interfaces et Systèmes Electrochimiques (LISE), 4 place Jussieu, F-75005, Paris, France.*

[2]*Safran Tech, rue des Jeunes Bois Châteaufort CS 80112, Magny les Hameaux, 78772, France.*

[3]*Sorbonne Université, CNRS, Laboratoire de Réactivité de Surface (LRS), UMR 7197, F-75005 Paris, France.*

[&] Present address: *Department of Chemistry, University of Illinois at Urbana−Champaign, Urbana, IL 61801, USA.*

Corresponding authors:

*vincent.vivier@sorbonne-universite.fr (Dr. Vincent Vivier)

**carlos.sanchez@sorbonne-universite.fr (Dr. Carlos M. Sánchez-Sánchez)

Abstract

The key improvement of the corrosion resistance of metals requires understanding and resolving the electrochemical reactions involved at the local scale. Here, we present the use of the pumped-micropipette delivery/substrate collection (Pumped-MD/SC) mode of scanning electrochemical microscopy (SECM) to monitor the oxygen reduction reaction (ORR) during corrosion of an Aluminum (Al) / Copper (Cu) galvanic coupled electrode, a model system of copper-rich aluminum alloys. In this case, the micropipette scans the substrate electrode pumping out a controlled flow of air-saturated electrolyte solution, which allows, through convective transport, to achieve high mass-transfer rates under steady-state conditions at the substrate electrode. The most relevant parameters in pumped-MD/SC mode were studied, it was demonstrated that the ORR current is linearly dependent on the injection flow rate. In contrast, the maximum ORR current was reached regardless of the tip-substrate distance (*d*) within the range of *L (d/ micropipette radius (a))* < 15, which represents a clear advantage in comparison with other modes of SECM. It was also proved that the ORR might take place on both Cu and Al electrodes depending on the applied potential. In addition, the pumped-MD/SC mode of SECM was successfully used for imaging large dimension surfaces with both high spatial and temporal resolution, as well as high imaging contrast thanks to the high mass-transfer rate of electroactive species achieved by forced convection. Moreover, relevant information to evaluate the effect of different corrosion inhibitors in solution such as $Ce_2(SO_4)_3$ and Li_2CO_3 on ORR was provided by individually addressing the substrate electrode in static pumped-MD/SC mode. It was demonstrated that only $Ce_2(SO_4)_3$ played the role of cathodic inhibitor through the formation of a Ce^{3+} oxide/hydroxide precipitate on the substrate electrode during ORR, which was confirmed by SEM and EDX analysis.

Keywords: Galvanic corrosion; oxygen reduction reaction; scanning electrochemical microscopy; micropipette

Graphical Abstract:

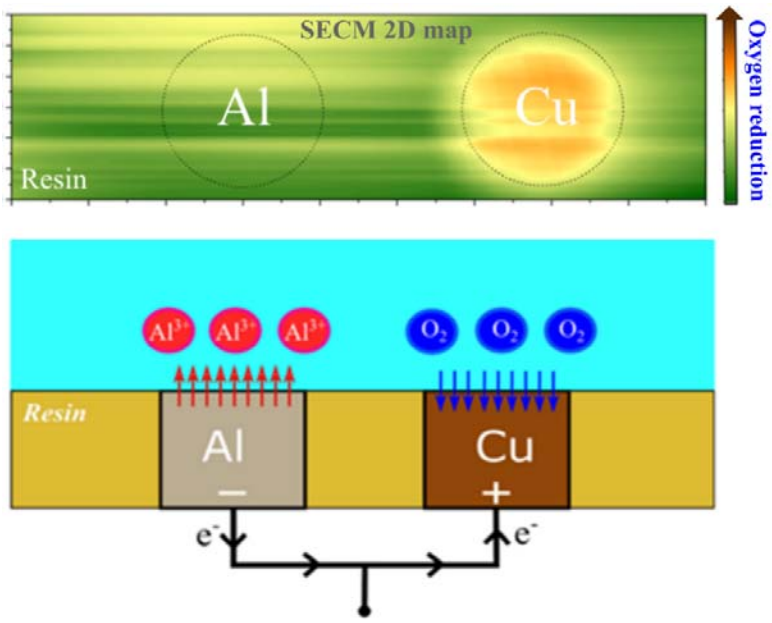

1. Introduction

Most bare metals suffer from spontaneous degradation reactions in the atmosphere and aqueous environments [1]. It is documented that billions of dollars are lost every year due to the corrosion of metals and alloys in many sectors [2]. The active corrosion of metals occurs dynamically by forming local micro-galvanic cells where some areas act as the anode, dissolving the metal, and other regions act as the cathode, where oxygen or/and water are reduced. In fact, improving the corrosion resistance of metals requires a deep understanding of the electrochemical reactions driving corrosion at the anode and cathode sites. This goal cannot be achieved by conventional electrochemical techniques such as potentiometric polarization curves, electrochemical impedance spectroscopy, and electrochemical noise analysis, which are unable to provide locally resolved data. This makes difficult to identify individual corrosion mechanism sites, and it requires probe-based techniques to locally resolve the electrochemical processes taking place. Ex situ spectroscopic techniques have been suggested to visualize physicochemical processes on metals surfaces [3,4]. However, mapping corrosion of metals at the micro- /nano-scale remains challenging due to lack of effective analytical tools. In the past decades, the multi-functional scanning electrochemical microscopy (SECM), which is considered as one of the few in situ/operando electrochemical techniques available for studying the electrode/electrolyte interface [5], demonstrated its capability to resolve electrochemical processes in the micro and lower scale ranges [6].

SECM [7] is based on the steady-state diffusion-controlled regime provided by either an ultramicroelectrode (UME) or a micropipette and was applied to visualize electrochemical processes on a wide range of metals using different modes [8]. In particular, tremendous efforts have been done to visualize the anodic sites on metal surfaces utilizing both amperometric and potentiometric probes with high special resolution. Iron (Fe^{2+}) [9,10], Nickel (Ni^{2+}) [11], Copper (Cu^{2+}) [12,13], Magnesium (Mg^{2+}) [14,15,16], and Zinc (Zn^{2+}) [17] ions flux coming out from the anodic sites were successfully monitored. On the other hand, the cathodic sites were also mapped mainly by the redox competition (RC) and tip generation/substrate collection (TG/SC) modes of SECM to monitor O_2 reduction reaction (ORR) [10,18,19,20,21,22], and the substrate generation/tip collection (SG/TC) mode of SECM to monitor H_2 evolution [23,24], respectively. However, the visualization of cathodic sites based on amperometric probes either by the RC or TG/SC modes present several limitations. For example, the local pH at the electrode surface might be modified when the SECM tip is biased to generate or reduce the oxygen at the SECM

probe. This is due to the release of either protons or hydroxide ions within the tip-substrate gap. It was demonstrated that a pH of 10 can be reached locally [21], which can induce a significant change in the electrochemical properties of the investigated metal and even may lead to pits generation as reported in the case of aluminium [25]. An additional limitation on amperometric probes is associated with the electrodeposition at the SECM probe of metal ions such as Fe^{2+}, Ni^{2+}, or Cu^{2+}released from the anodic sites of the substrate while reducing the oxygen, which provokes misinterpretation of the experimental results. Thus, different micropipette-based approaches have been developed to overcome those limitations observed in studying the role of oxygen on metal surfaces either in corrosion, bio-applications or electrocatalysis. Engstrom in 1984 [26] presented one of the first attempts of using micropipettes for mapping the electrochemical activity of an electrode. Micropipettes having diameters of less than 1 μm were filled with a solution of an ionic redox mediator and positioned over a Pt electrode. Ions come out of the micropipette by migration, which only allowed transient faradaic currents to be collected on the substrate electrode at a very small tip-substrate distance. More recently, the micropipette delivery/substrate collection (MD/SC) mode has demonstrated its utility for studying electrochemical reactions of neutral species that cannot be electrochemically generated such as methanol [27], chloroform [28] and formic acid [29,30]. The diffusion of those species across a liquid-liquid interface between two immiscible electrolyte solutions allows releasing of methanol, chloroform or formic acid from the micropipette into the bulk solution at a controlled rate. However, the rate of electroactive species coming out from the micropipette is still very limited. Thus, convective transport to release electroactive species from micropipettes represents an attractive approach for achieving enhanced and variable mass-transfer rates under steady-state conditions. Unwin's group in Warwick is one of the pioneers in developing that approach thanks to the microjet electrode (MJE) [31], where a jet of solution from a micropipette hits a disc shape UME. Controlling the solution release rate is the most critical point, being gravity-feed [32] and peristaltic pump-feed [33] injection the initial methods used for delivering the solution out of the micropipette within the range of (μL/s). However, the accumulation of solution in the cell forces to reduce the pumping flow rate, which needs to be placed in the range of (nL/s) for not producing any significant variation of volume within the cell during SECM activity evaluation. Bard's group set up a powerful dispensing micropipette together with a ring-shape electrode [34], which dispenses very small amounts of solution (pL), while simultaneously monitoring the electrochemical response collected at the substrate and at the ring tip electrode. Nevertheless, mostly SECM images of outer-sphere redox mediators released by convection from micropipettes have been reported [33,34] and no

applications to evaluate inner-sphere reactions can be found in the literature. So far, only biological SECM imaging of horseradish peroxidase protein microarray in continuous nanoflow has been reported [35].

The pumped-micropipette delivery/substrate collection (pumped-MD/SC) mode of SECM was already successfully employed in pitting corrosion studies [36,37,38,39], where aggressive anions such as chloride were released from the micropipette in close vicinity of a stainless-steel electrode. However, no SECM imaging was reported in those cases. Thus, we present herein the pumped-MD/SC mode to monitor the inner-sphere ORR on an Al/Cu galvanic electrode, a model system often used to simulate the corrosion of copper-rich aluminum alloys [40,41,42,43]. Thus, Al/Cu galvanically coupled substrate is investigated by locally releasing O_2 from an air-saturated solution using the pumped-MD/SC mode of SECM with and without the presence of two different corrosion inhibitors in the bulk solution (Ce^{3+} and Li^{+}).

2. Experimental

2.1 Al/Cu galvanic electrode

The aluminum (Al)/copper (Cu) galvanic cell was prepared by embedding Al and Cu wires of 1 mm in diameter in an epoxy resin to produce a flat surface with the two materials surrounded by an electrical insulator. Al (supplied by Goodfellow) with a purity of 99.99% and Cu (supplied by Goodfellow) with a purity of 99.9% were employed. The Cu and Al wires (separated by 1 cm) were first placed in a cylindrical mold that was filled with a mixture of the resin and hardener (*Epofix*). The resin was left for 12 h to harden at room temperature. A smooth and flat surface was obtained by grinding with SiC paper. Further polishing was carried out using alumina slurries with different grain sizes from 1.0 to 0.05 μm.

2.2 Glass micropipette fabrication

Micropipettes were prepared by pulling single barrel borosilicate capillaries with filament, O.D.: 1.0 mm and I.D.: 0.5 mm and length 15 cm (World Precision Instruments) using a CO_2 laser-based puller P-2000 from Sutter Instrument Co. Micropipettes with an internal opening diameter of c.a. 15 μm were fabricated applying the following pulling parameters: line 1: heat = 375, filament = 3, velocity = 11, delay = 180. The micropipette opening diameter was

measured using an optical metallographic microscope BA310MET-H (Motic Co.). Then, glass micropipettes were loaded with an air-saturated electrolyte solution and connected to a syringe pump before starting the ORR evaluation by SECM.

2.3 Scanning electrochemical microscopy (SECM)

A CHI 920D (CH Instruments) microscope in the pumped micropipette delivery/substrate collection (pumped-MD/SC) mode was used in all cases. In this mode configuration, a borosilicate micropipette with an internal opening diameter of 15 μm replaces the UME to locally deliver the analyte of interest (O_2) in the vicinity of the electrode surface. The top-end of the glass micropipette was connected through a PTFE capillary (I.D. 1.06 and O.D. 1.68 mm) to a 300 μL Terumo® syringe filled with an air-saturated 0.1 M Na_2SO_4 solution. A KD Scientific® syringe pump (model 100) was used to release the solution from the syringe into the micropipette and subsequently at the vicinity of the electrode surface at a controlled flux rate, as sketched in **Figure 1A**. An electrochemical cell made of Teflon with an 8 mm diameter aperture was used to define the available area of the substrate electrode in contact with the solution. Both metals present within the Al/Cu galvanic couple were connected together acting as one single working electrode (see **Figure 1A**). Ag/AgCl/3 M KCl in a Luggin capillary and a Pt wire (0.5 mm in diameter) were used as a reference and counter electrodes, respectively. The same solution contained within the glass micropipette, but without the presence of O_2 (Argon-saturated), was used in the electrochemical cell.

The precise positioning of the micropipette was performed by an approach curve in the Z axis at a low speed (1 μm/s). This approach was performed from air to a point of contact on the substrate electrode in an empty SECM cell (see **Figure 1B)**, meanwhile the solution was pumped through the micropipette at a high rate (100 μL/h). The contact point was established by physical contact between the meniscus formed at the apex of the micropipette and the insulating part of the substrate electrode in the air. This technique avoids damaging the micropipette integrity and allows high sensitivity to position the micropipette in the close vicinity of the substrate. The micropipette-substrate distance was set up at a constant value (d) represented as normalized distance ($L = d/a$), where (a) corresponds to the micropipette radius (a = 7.5 μm). Finally, the electrochemical cell was filled up with the Argon-saturated electrolyte. Three types of SECM experiments are reported here: *i*) SECM single line scan, *ii*) SECM imaging and *iii*) SECM activity quantification by chronoamperometry.

i) SECM line scan and *ii*) *SECM imaging*: The Al/Cu galvanic electrode was held constant at a proper potential value to evaluate ORR activity; meanwhile, the micropipette scans the substrate electrode pumping out a controlled flow of air-saturated 0.1 M Na_2SO_4 solution. Then, the oxygen reduction current produced at the substrate during the micropipette scan in the X-Y plane was recorded as a function of micropipette position and plotted as either one single SECM line scan or the addition of successive line scans covering a larger area of the substrate electrode and giving as a result a SECM image. An argon blanket was kept over the Argon-saturated 0.1 M Na_2SO_4 bulk solution during the experiment to keep the solution free from atmospheric oxygen. In the case of the SECM line scan, the injection flow rate was varied between 45 and 142 µL/h and the micropipette-substrate distance between 30 and 260 µm. In contrast, in the case of SECM imaging, the injection flow rate was 45 µL/h and the micropipette-substrate distance 50 µm.

ii) SECM activity quantification by chronoamperometry. This experiment was conducted with the micropipette in static mode by individually addressing the Cu spot at the substrate. The micropipette was placed at the center of the Cu spot at a micropipette-substrate distance of 30 µm. Then, a chronoamperometry for 3000 s keeping the potential constant in an active region for ORR (-0.4 V vs Ag/AgCl/3 M KCl) at the Cu spot was carried out. Firstly, the substrate background current was collected during approx. 250 s; meanwhile, the micropipette was not delivering any O_2 in the solution ($I_{background}$) because the syringe pump was turned off. Secondly, the syringe pump was turned on and an air-saturated 0.1 M Na_2SO_4 solution was released from the micropipette for approx. 250 s. Then, the substrate current collected corresponds to the ORR activity at the Cu spot (I_{ORR}) under steady-state conditions. This Off/On process was repeated for 2 more cycles and finally, the syringe pump was turned off again before the end of the chronoamperometry experiment. The net ORR current (ΔI) associated with the activity of the Cu spot was calculated for each Off/On cycle from the difference between the reduction current collected in the presence and the absence of O_2 ($\Delta I = I_{ORR} - I_{background}$) either in the absence or the presence of corrosion inhibitors in solution.

2.4 Energy-Dispersive X-ray (EDX)/ Scanning Electron Microscope (SEM)

The morphology and the chemical composition of the investigated Cu electrode before and after the corrosion inhibitors action were evaluated by Scanning Electron Microscopy (Ultra 55 SEM from ZEISS) and Energy-Dispersive X-ray Spectroscopy (SEM-EDX) analysis with

a detector Everhart Thornley SE2 (operating with a 10 kV electron beam and 5.5 mm aperture) and a spectrometer Quantax from Bruker. The binding energy was calibrated using a Cu disk.

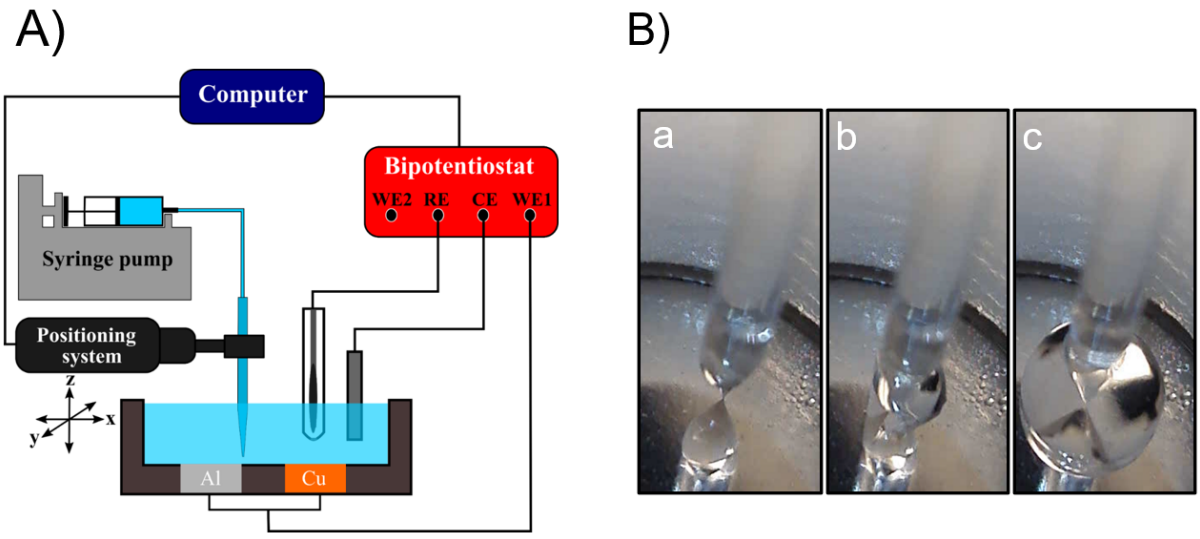

Figure 1. *A- Sketch of the Pumped-MD/SC SECM set up. B- Photos showing the different stages of the approach curve for micropipette positioning: a- the micropipette is pumping solution, but it is not in contact with the substrate electrode, b- the contact point is reached between the micropipette and the substrate electrode surface, c- an increasing substrate electrode surface is covered by solution pumped from the micropipette after reaching the contact point.*

3. Results and discussion

Polarization measurements were individually performed on Cu and Al electrodes, and are presented in **Figure 2A**. As expected, the corrosion potential of Cu is more positive than the Al electrode, pointing out that when the Cu and Al wires are electrically connected to form a galvanic couple in solution, Cu is acting as the cathode and Al as the anode of the corrosion process. Based on those polarization experiments, a selected potential of -0.4 V vs Ag/AgCl/3 M KCl, which is considered anodic for Al and cathodic for Cu electrode (as sketched in **Figure 2B**), was applied to the Al/Cu galvanic electrode during the SECM experiments in the Pumped-MD/SC mode.

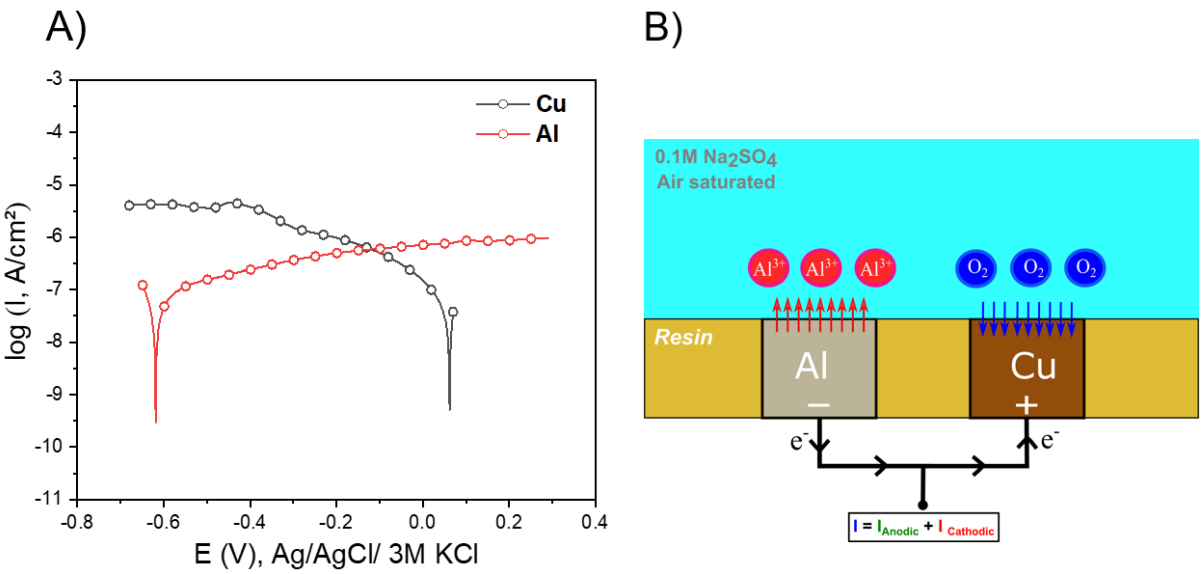

Figure 2. *A- Tafel potentiodynamic polarization curves of Cu and Al electrodes in 0.1 M Na_2SO_4 solution. Scan rate: 1 mV s^{-1}. B- Sketch illustrating the galvanic corrosion between Cu and Al electrodes.*

The first series of experiments with the Pumped-MD/SC mode of SECM was performed to investigate the effect of the solution injection flow rate on the oxygen reduction current collected at the substrate electrode. For that purpose, the glass micropipette was set at a constant tip-substrate distance of 30 µm (L = 4) and a potential of -0.4 V *vs* Ag/AgCl/3 M KCl was applied to the Al/Cu galvanic electrode. Then, consecutive line scans in the X axis were performed over the Al/Cu galvanic electrode varying the injection flow rate from 45 to 142 µL/h, as shown in **Figure 3A**. A significant increase in substrate current appears when the micropipette scans the Cu electrode, which is attributed to the ORR. Moreover, the substrate background current when the micropipette is scanned over the insulating resin is about 200 nA, which is almost identical to the collected current displayed over the Al electrode for all solution injection flow rates studied. This underlines that a higher overpotential needs to be applied on Al than on Cu electrode to perform ORR, which is in agreement with the polarization curves presented in **Figure 2A**. On the other hand, a significant increase in collected current was measured over the Cu electrode when increasing the solution injection flow rate. Such a variation can be explained by the electrochemical reduction of oxygen released from the micropipette, which takes place on the Cu electrode. **Figure 3B** illustrates the linear relationship of the oxygen reduction current as a function of the solution injection flow rate, which is due to the variation of oxygen mass transfer at the Cu electrode surface. Indeed, such

an experiment can be explained by the forced convection, which results in a decrease of the diffusion layer thickness when the solution flow rate increases.

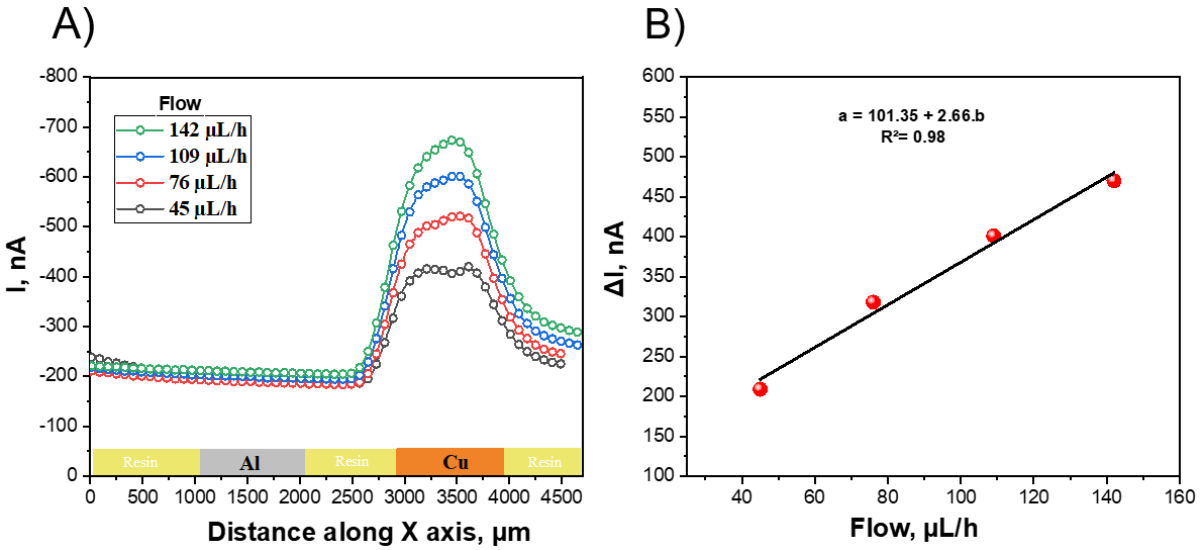

Figure 3. *A- Line scans recorded over the Al/Cu galvanic electrode by Pumped-MD/SC mode of SECM under various solution injection flow rates. The substrate was polarized at -0.4 V vs Ag/AgCl/3 M KCl in an oxygen-free 0.1 M Na_2SO_4 solution. Tip: micropipette inner diameter of 15 µm filled with an air saturated 0.1 M Na_2SO_4 solution; tip-substrate distance: 30 µm; tip scan rate: 20 µm/s. B- Maximum net ORR current (ΔI) measured when the tip is above the Cu electrode as a function of the solution injection flow rate.*

The effect of the tip-substrate distance on the oxygen reduction current collected at the substrate electrode was studied by the Pumped-MD/SC mode of SECM performing consecutive line scans in the X axis (**Figure 4A**). For that purpose, the injection flow rate was set at 45 µL/h and a potential of -0.4 V *vs* Ag/AgCl/3 M KCl was applied to the Al/Cu galvanic electrode. These line scans show that the collected current over the insulating resin and Al electrode are basically independent of the tip-substrate distance because no ORR is taking place there. In contrast, the collected current at the Cu electrode is significantly higher than the background current and presents two different behaviors depending on the tip-substrate distance value. **Figure 4B** illustrates the relationship of the oxygen reduction current as a function of tip-substrate distance. Interestingly, a turning point is located at 110 µm ($L \approx 15$), above which the collected current progressively decreases when increasing the tip-substrate distance, but below which the current becomes tip-substrate distance independent and reaches a constant maximum. Such behavior is in agreement with the control of the diffusion layer thickness reported by Chin and Tsang [44] in the case of mass transfer to an impinging jet electrode.

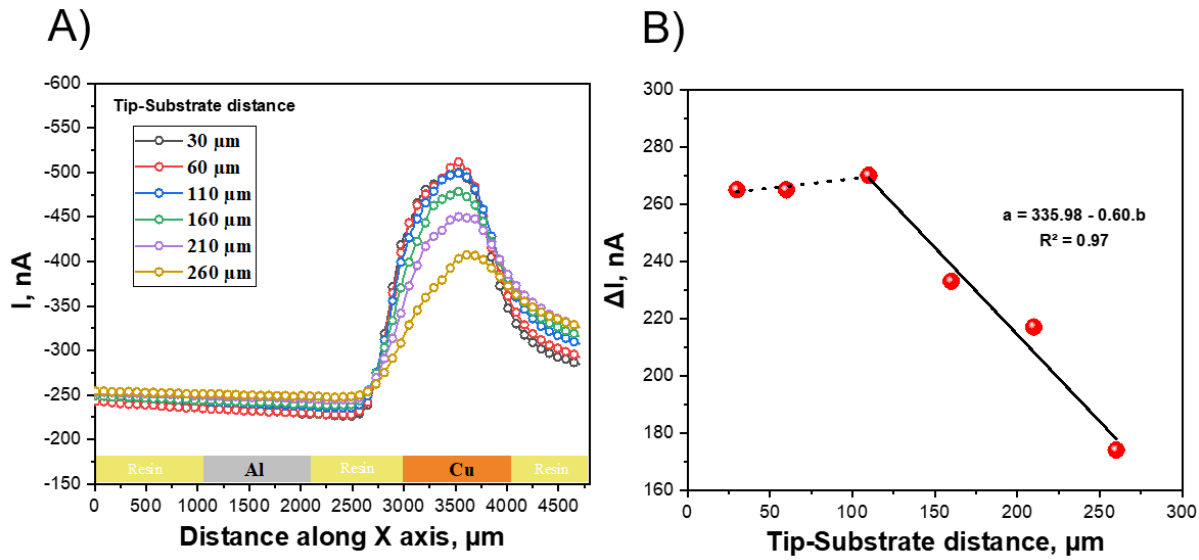

Figure 4. *A- Line scans recorded over the Al/Cu galvanic electrode by Pumped-MD/SC mode of SECM as a function of the tip-substrate distance. The substrate was polarized at -0.4 V vs Ag/AgCl/3 M KCl in an oxygen-free 0.1 M Na_2SO_4 solution. Tip: micropipette inner diameter of 15 µm filled with an air saturated 0.1 M Na_2SO_4 solution; injection flow rate: 45µL/h; tip scan rate: 20 µm/s. B- Maximum net ORR current (ΔI) measured when the tip is above the Cu electrode as a function of the tip-substrate distance.*

The effect of the applied potential at the substrate electrode on the oxygen reduction current collected was studied by the Pumped-MD/SC mode of the SECM performing a line scan in the X axis (**Figure 5**). For that purpose, the solution injection flow rate was set at 45 µL/h and the tip-substrate distance at 30 µm (L = 4). According to the polarization curves presented in **Figure 2A**, it is expected that the ORR takes place on both Al and Cu electrodes at an applied potential of – 0.7 V vs Ag/AgCl/ 3 M KCl. Thus, the background current measured above the resin is more negative compared to the one measured in the previous line scans (Figures 3A and 4A) performed at less cathodic potential (-0.4 V vs Ag/AgCl/ 3 M KCl). On the other hand, a significant current was measured on both the Al and Cu electrodes, but larger values were collected above the Cu electrode, which demonstrated its higher reactivity towards the ORR. This fact further confirmed that the Pumped-MD/SC mode of the SECM enables to sense the local reactivity of the electrode by directly releasing the redox reactant (**Figure 5**). Moreover, it is demonstrated a relevant role of the applied potential on the oxygen reduction current, since the maximum net collected current at -0.7 V vs Ag/AgCl/ 3 M KCl (**Figure 5**) is double than that collected under the same experimental conditions, but at -0.4 V vs Ag/AgCl/ 3 M KCl (grey plot in **Figure 4A**). This fact is directly controlled by the number of electrons transferred during the ORR, which varies as a function of the applied potential and the chemical nature of the studied electrode.

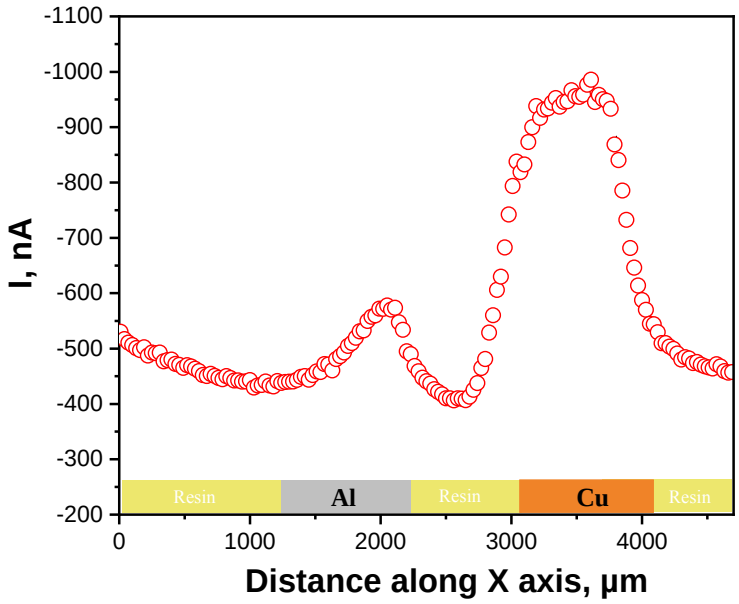

Figure 5. *Line scan recorded over the Al/Cu galvanic electrode by Pumped-MD/SC mode of SECM. The substrate was polarized at -0.7 V vs Ag/AgCl/3 M KCl in an oxygen free 0.1 M Na_2SO_4 solution. Tip: micropipette inner diameter of 15 µm filled with an air saturated 0.1 M Na_2SO_4 solution; tip-substrate distance: 30 µm; injection flow rate: 45µL/h; tip scan rate: 20 µm/s.*

Finally, it was also demonstrated that the Pumped-MD/SC mode of the SECM can be a useful tool for imaging the cathodic regions during corrosion of a rather large size sample. **Figure 6A** shows the optical microscope image of the Al/Cu galvanic electrode and **Figure 6B** the corresponding SECM image performed at an applied potential of – 0.4 V *vs* Ag/AgCl/ 3 M KCl with a micropipette set at a tip-substrate distance of 50 µm ($L \approx 7$) pumping out solution at a flow rate of 45 µL/h. This SECM image only allows to identify the Cu electrode location, since the Al electrode is not active for ORR at the applied potential used. For this reason, a dotted circle has been drawn in **Figure 6B** to identify the Al electrode location. This result can be easily correlated with the previous SECM line scan results reported in **Figures 3A** and **4A**, which show that the electrochemical reduction of oxygen takes only place on the Cu electrode for an applied potential of -0.4 V *vs* Ag/AgCl/ 3 M KCl. Moreover, it can be also seen that a high-resolution image was obtained, being the resolution controlled by the inner diameter of the micropipette used for imaging and its distance to the substrate. Such a behavior is similar to what was already reported for the spatial resolution of the conventional SECM [45]. Nevertheless, the high mass-transfer of the reactant controlled by forced convection reached in the pumped-MD/SC mode represents one of its main advantages for imaging versus other

generation/collection modes. In particular, the maximum collected current at the substrate is obtained regardless the tip-substrate distance within the range of $L < 15$ (**Figure 4**), which avoids working in close vicinity between the micropipette and the substrate electrode during SECM imaging. This feature is very interesting for imaging large size samples with a low risk of crashing the micropipette.

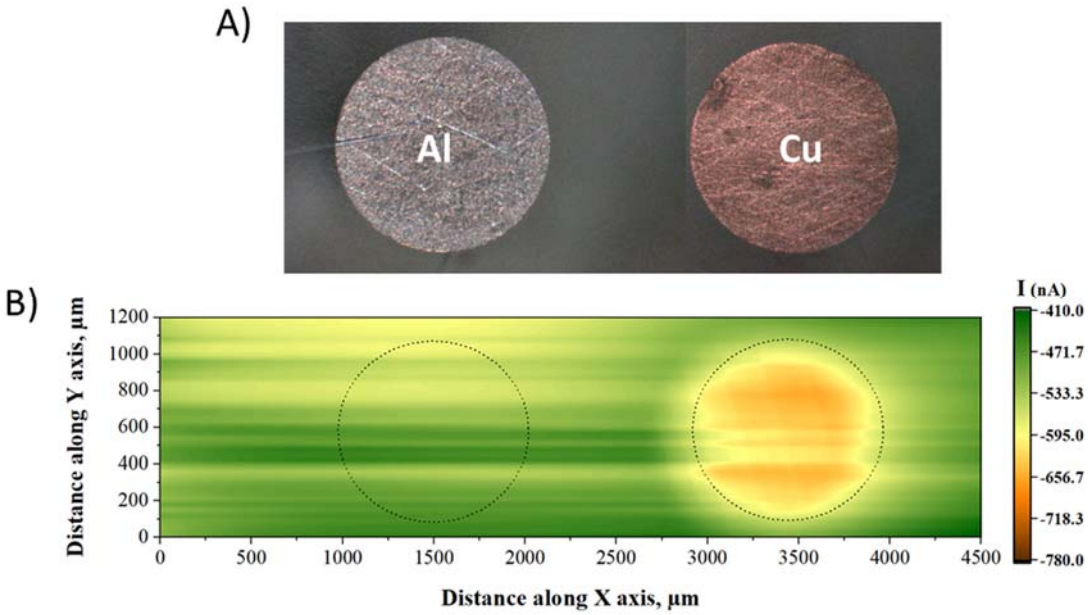

Figure 6. *A- Optical microscope image of the Al/Cu galvanic substrate electrode. B- SECM image by Pumped-MD/SC mode based on the collected current generated on an Al/Cu galvanic electrode. The substrate was polarized at -0.4 V vs Ag/AgCl/3 M KCl in an oxygen free 0.1 M Na_2SO_4 solution. Tip: micropipette inner diameter of 15 µm filled with an air saturated 0.1 M Na_2SO_4 solution; tip-substrate distance: 50 µm; injection flow rate: 45µL/h; tip scan rate: 20 µm/s.*

Figure 7A schematically describes the ORR activity quantification by chronoamperometry at the Cu electrode using the Pumped-MD/SC mode of the SECM. This was conducted with the micropipette individually addressing the Cu electrode of the substrate in static mode and performing a chronoamperometry, which is divided into different zones depending on whether the pump to release the solution from the micropipette is turned On or Off. In particular, the ORR activity quantification by SECM was used herein for evaluating the impact of two different corrosion inhibitors in solution (Ce^{3+} and Li^{+}). In these experiments, addition in the bulk solution of either cerium sulphate ($Ce_2(SO_4)_3$) [46] or lithium carbonate (Li_2CO_3) [47,48], which are known as cathodic and anodic inhibitors, respectively, were studied. **Figure 7B** shows the ORR quantification performed in the absence of any corrosion inhibitor in solution. Thus, the micropipette released air saturated 0.1 M Na_2SO_4 solution when the syringe pump

was turned on, meanwhile the electrochemical cell contained an oxygen-free 0.1 M Na_2SO_4 solution. Three Off/On cycles were repeated during the chronoamperometry. The net ORR current (ΔI) associated with the activity of the Cu spot was calculated for each consecutive Off/On cycle and it is stated in **Figure 7B** (-226, -210, and -171 nA). A slight decrease in net current is observed from Off_1/On_1 to Off_3/On_3 cycle, which is probably related to some deactivation of the ORR due to the Cu electrode aging during the long duration of the chronoamperometry (3000 s).

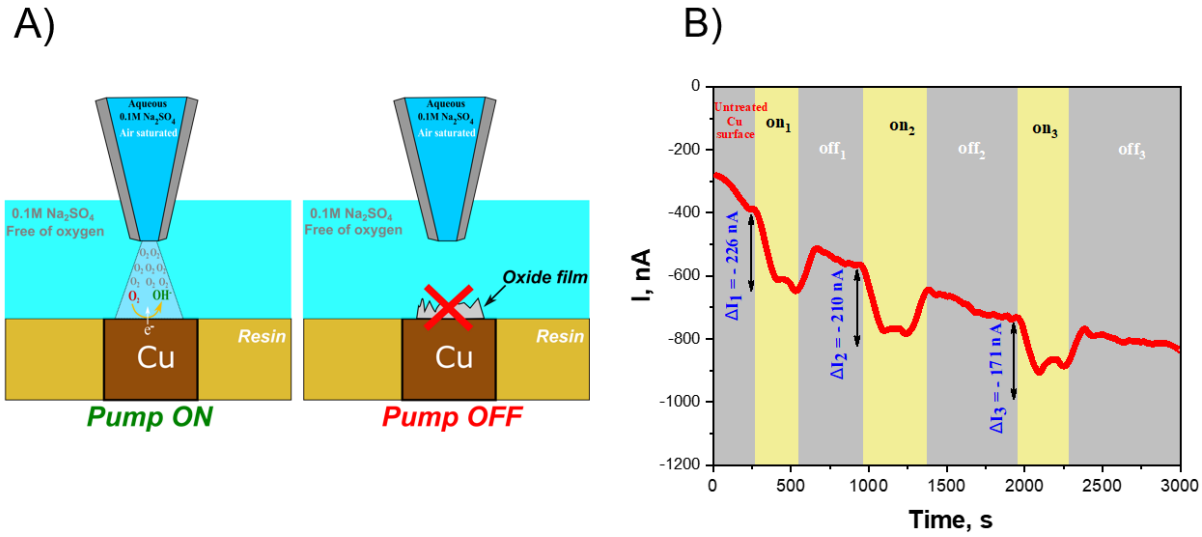

Figure 7. *A- Sketch of the ORR activity quantification setup on copper electrode by Pumped-MD/SC mode of SECM. B- ORR chronoamperometry activity quantification by SECM performed on copper electrode immersed in an oxygen free 0.1 M Na_2SO_4 solution. Applied potential: -0.4 V vs Ag/AgCl/3 M KCl. Tip: micropipette inner diameter of 15 µm filled with an air saturated 0.1 M Na_2SO_4 solution; tip-substrate distance: 30 µm; Injection flow rate: 45µL/h. (ΔI) represents the net ORR current in each Off/On cycle.*

Figure 8A describes an analogous sketch to the one previously presented in **Figure 7A** for the ORR activity quantification, but adding 0.1% wt. Li_2CO_3 into the bulk solution. In this case, **Figure 8B** shows the ORR quantification on the Cu electrode performed in the presence of Li^+ in solution acting as a corrosion inhibitor. The net ORR current (ΔI) from each consecutive Off/On cycle stated in **Figure 8B** exhibits a slight decrease (-505, -400 and -424 nA), which is very similar to the one observed in the absence of Li^+ in **Figure 7B**. This highlights that Li_2CO_3 doesn't play any role as cathodic inhibitor, which is in agreement with previous literature proposing that Li^+ inhibits the corrosion process at the anodic poles via the rearrangement of the surface oxide film as discussed for aluminum alloys [47,48].

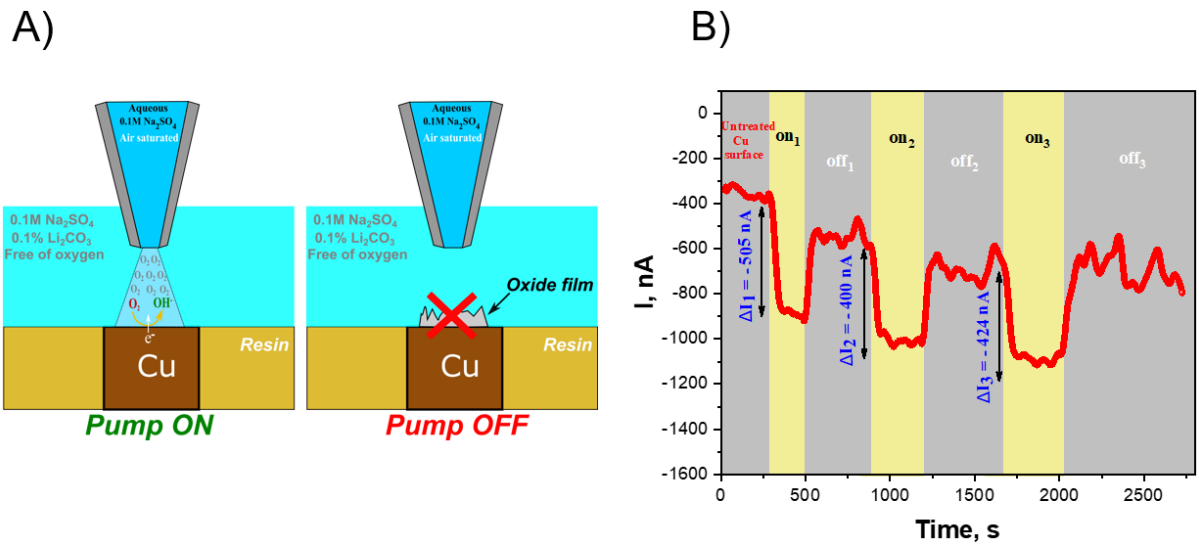

Figure 8. *A- Sketch of the ORR activity quantification setup on copper electrode in the presence of Li_2CO_3 inhibitor by Pumped-MD/SC mode of SECM. B- ORR chronoamperometry activity quantification by SECM performed on copper electrode immersed in an oxygen free 0.1 % wt. Li_2CO_3 and 0.1 M Na_2SO_4 solution. Applied potential: -0.4 V vs Ag/AgCl/3 M KCl. Tip: micropipette inner diameter of 15 µm filled with an air saturated 0.1 M Na_2SO_4 solution; tip-substrate distance: 30 µm; Injection flow rate: 45µL/h. (ΔI) represents the net ORR current in each Off/On cycle.*

Figure 9A describes an analogous sketch to the one previously presented in **Figures 7A** and **8A** for the ORR activity quantification, but adding 0.1% wt. $Ce_2(SO_4)_3$ into the bulk solution. In this case, **Figure 9B** shows the ORR quantification on the Cu electrode performed in the presence of Ce^{3+} in solution acting as a corrosion inhibitor. Chronoamperometry in **Figure 9B** displays a very different behavior in the presence of Ce^{3+}. The net ORR current (ΔI) from each consecutive Off/On cycle stated in **Figure 9B** exhibits a very sharp drop with time (-420, -94, and -19 nA), which points out that the ORR rate at the Cu electrode significantly decreases due to the inhibition action of Ce^{3+} in solution. Then, chemical composition analysis by EDX was carried out on the surface of the Cu electrode after the chronoamperometry experiment reported in **Figure 9B**, in order to identify any potential deposition produced at the Cu electrode surface. SEM image and EDX analysis in **Figure 10A** show a heterogeneous surface with cerium and oxygen homogeneously distributed all over the Cu surface, respectively. Thus, chemical mapping of Ce and O by EDX analysis shown in **Figure 10A** demonstrated the formation of a Ce^{3+} oxide and/or hydroxide inhibition layer at the Cu electrode surface during ORR, which is responsible of the sharp drop in the net ORR current observed in **Figure 9B**. These results prove the role of cathodic inhibitor of Ce^{3+}.

It is well stablished in the literature that most metals such as Cu present a dual reaction pathway during ORR, where the competition between the $2e^-$ and $4e^-$ reaction pathways (Equations 1 and 2, respectively) mainly depends on the applied potential [49]. Thus, the ORR at the Cu electrode in both cases leads to an increase of the local pH via the consumption of protons, as shown in Equations 1 and 2. Moreover, it has been reported that a pH of 10 can be easily reached during ORR on the Cu electrode [50,51]. Thus, we propose the local precipitation of Ce^{3+} in alkaline pH as a form of oxide and/or hydroxide due to the increase of the local pH at the Cu electrode surface during ORR (Equations 3, 4 and 5). The presence of Ce^{3+} oxide/hydroxide on the investigated Cu electrode was further confirmed by SEM and EDX analysis shown in **Figure 10A**. The different domains of pH where Ce^{3+} species are soluble and stable are well stablished in the literature. **Figure 10B** shows the Ce^{3+} species distribution diagram as a function of solution pH. In principle, Ce^{3+} species in solution are stable at a pH 7, *i.e.*, at a pH value similar to the initial bulk solution. However, Ce^{3+} species precipitate to form $Ce(OH)_3$ in alkaline solution (pH > 9), via reaction 5.

$$O_2 + 2H^+ + 2e^- \rightarrow H_2O_2 \qquad \text{Eq. 1}$$

$$O_2 + 4H^+ + 4e^- \rightarrow 2H_2O \qquad \text{Eq. 2}$$

$$Ce^{3+} + OH^- \rightarrow Ce(OH)^{2+} \qquad \text{Eq. 3}$$

$$Ce^{3+} + 2OH^- \rightarrow Ce(OH)_2^+ \qquad \text{Eq. 4}$$

$$Ce^{3+} + 3OH^- \rightarrow Ce(OH)_3\downarrow \qquad \text{Eq. 5}$$

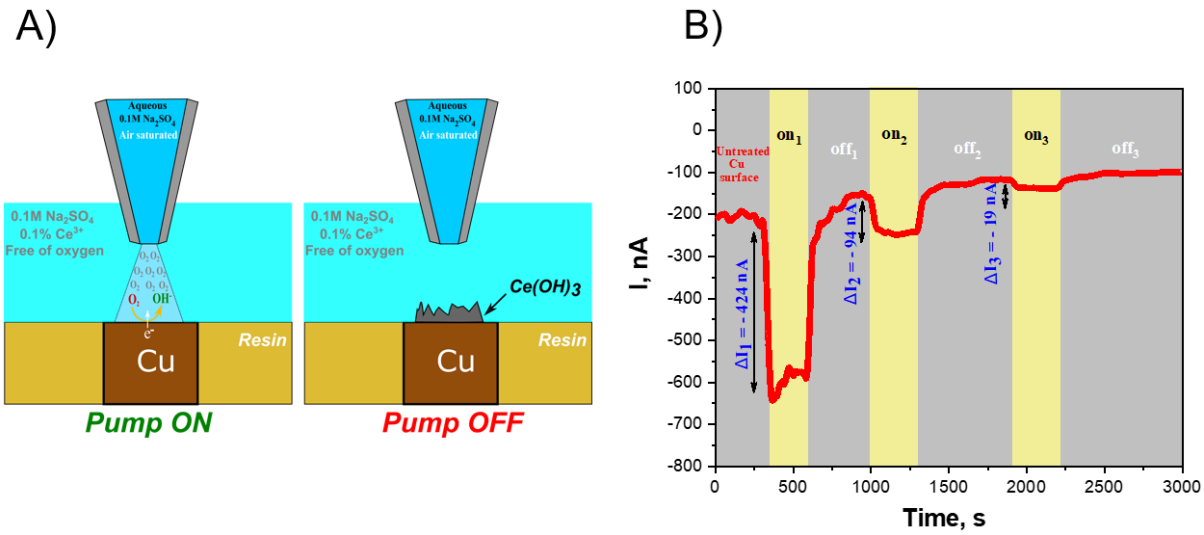

Figure 9. *A- Sketch of the ORR activity quantification setup on copper electrode in the presence of $Ce_2(SO_4)_3$ inhibitor by Pumped-MD/SC mode of SECM. B- ORR chronoamperometry activity quantification by SECM performed on copper electrode immersed in an oxygen free 0.1 % wt. $Ce_2(SO_4)_3$ and 0.1 M Na_2SO_4 solution. Applied potential: -0.4 V vs Ag/AgCl/3 M KCl. Tip: micropipette inner diameter of 15 µm filled with an air saturated 0.1 M Na_2SO_4 solution; tip-substrate distance: 30 µm; Injection flow rate: 45µL/h. (ΔI) represents the net ORR current in each Off/On cycle.*

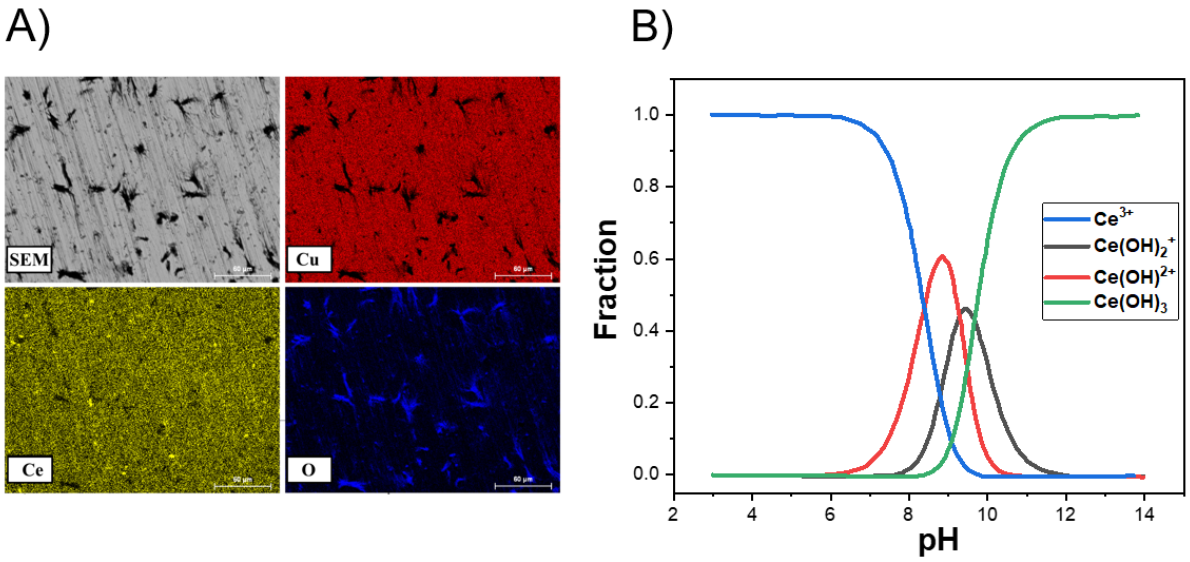

Figure 10. *A- SEM image and chemical mapping of Cu, Ce and O by EDX performed on the Cu electrode surface after the ORR activity quantification by chronoamperometry using the Pumped-MD/SC mode of the SECM was carried out with the presence of ($Ce_2(SO_4)_3$) in solution. B- Ce^{3+} species distribution diagram as a function of the solution pH.*

4. Conclusions

Forced convection transport to release electroactive species from a micropipette have represented an attractive, but difficult, approach for achieving enhanced and variable mass-transfer rates under steady-state conditions from the beginning of SECM development. Thus, we present a step forward, the pumped-micropipette delivery/substrate collection (pumped-MD/SC) mode of SECM, which is applied here for monitoring ORR during corrosion on metal surfaces. This convective generation/collection mode presents a tremendous number of potential applications in corrosion and electrocatalysis studies, since allows to overcome most of the limitations present in other SECM modes. The pumped-MD/SC mode allows to study any soluble electroactive species, including charged and neutral species, and does not locally electrogenerate them, which avoids any local pH modification induced by the electrochemical generation of the reactant in the gap between the tip and the substrate electrode. Moreover, convection transport allows to enhance the SECM imaging contrast by taking advantage of the higher mass-transfer rate achieved in comparison with the conventional diffusion rate. In particular, we present herein a corrosion study for tracking cathode sites on Al/Cu galvanic electrode, a model system often used to simulate the corrosion of copper-rich aluminum alloys.

The effect on the ORR current collected at the substrate electrode of the most relevant parameters in pumped-MD/SC mode (solution injection flow rate, tip-substrate distance and applied potential) was studied here. Firstly, it was demonstrated that the ORR current is linearly dependent with the solution injection flow rate. Secondly, the maximum ORR current at the substrate was obtained regardless the tip-substrate distance within the range of $L < 15$, which avoids working in close vicinity between the micropipette and the substrate electrode during SECM imaging, allowing large dimension SECM images to be acquired. Thirdly, ORR takes place either on Cu or Al electrodes depending on the applied potential imposed.

Furthermore, the pumped-MD/SC mode of SECM was effectively used here for studying corrosion inhibition by ORR activity quantification. This was conducted with the micropipette individually addressing the Cu electrode of the substrate in static mode and performing a chronoamperometry, where the net ORR current corresponded to the difference between the current when the pump controlling the solution release from the micropipette was turned Off and the current when it was On. In particular, the effect of two different inhibitors (Li_2CO_3 and $Ce_2(SO_4)_3$) on the ORR at Cu electrode was studied. The Pumped-MD/SC mode of SECM was

able to prove that Li_2CO_3 doesn't play any role as cathodic inhibitor, but an important role of $Ce_2(SO_4)_3$ as cathodic inhibitor. This inhibition mechanism was based on the formation of a Ce^{3+} oxide/hydroxide precipitate on the Cu electrode surface during ORR, which was confirmed by SEM and EDX analysis. Interestingly, these results pave the way for the use of the Pumped-MD/SC mode of SECM not only to study ORR, but other redox species and inner-sphere reactions as well.

CRediT authorship contribution statement

Abdelilah Asserghine: Conceptualization, Methodology, Investigation, Data curation, Formal analysis, Validation, Visualization, Writing - original draft, Writing - review & editing. **Sophie Juillard**: Methodology, Formal analysis, Writing - review & editing. **Julie Ducrot**: Project administration, Formal analysis, Writing - review & editing, Funding. **Vincent Vivier**: Conceptualization, Data curation, Validation, Visualization, Formal analysis, Writing - review & editing. **Carlos. M. Sánchez-Sánchez**: Supervision, Project administration, Conceptualization, Data curation, Validation, Formal analysis, Writing - original draft, Writing - review & editing, Funding acquisition.

Declaration of Competing Interest

The authors declare that they have no known competing financial interests or personal relationships that could have appeared to influence the work reported in this paper.

Acknowledgements

The authors acknowledge the support of the Centre National de la Recherche Scientifique (CNRS). Dr. A. Asserghine is thankful to A. Z. Benbouzid for his comments and fruitful discussion. S. Juillard thanks Sorbonne Université for the PhD contract. This work was financially supported by Safran Tech.

References

[1] G. S. Frankel, Pitting corrosion of metals: a review of the critical factors, J. Electrochem. Soc. 145 (1998) 2186.

[2] R. Javaherdashti, How corrosion affects industry and life. Anti-Corros. Methods Mater. 47 (2000) 30–34.

[3] C. A. Melendres, Laser raman spectroscopy in studies of corrosion and electrocatalysis. Spectroscopic and diffraction techniques in interfacial electrochemistry. Springer, Dordrecht, 1990. 181-222.

[4] L. Bellot-Gurlet, D. Neff, S. Réguer, J. Monnier, M. Saheb, P. Dillmann, Raman studies of corrosion layers formed on archaeological irons in various media, Journal of Nano Research 8 (2009) 147.

[5] Y. Zhu, J. Wang, H. Chu, Y.-C. Chu, H. M., Chen, In situ/operando studies for designing next-generation electrocatalysts, ACS Energy Lett. 5 (2020) 1281.

[6] D. Polcari, P. Dauphin-Ducharme, J. Mauzeroll. Scanning electrochemical microscopy: a comprehensive review of experimental parameters from 1989 to 2015, Chem. Rev. 116, 22 (2016) 13234.

[7] A. J. Bard, M. V. Mirkin, eds., Scanning Electrochemical Microscopy, 2nd edition, CRC Press, Boca Raton, 2012.

[8] N. A. Payne, L. I. Stephens, J. Mauzeroll. The application of scanning electrochemical microscopy to corrosion research, Corrosion 73 (2017) 759.

[9] C. F. Dong, H. Luo, K. Xiao, X. G. Li, Y. F. Cheng, In situ characterization of pitting corrosion of stainless steel by a scanning electrochemical microscopy, J. Mater. Eng. Perform. 21 (2012) 406.

[10] A. C. Bastos, A. M. Simoes, S. González, Y. González-Garcia, R. M. Souto, Imaging concentration profiles of redox-active species in open-circuit corrosion processes with the scanning electrochemical microscope, Electrochem. Commun. 6 (2004) 1212.

[11] D. Ruhlig, H, Gugel, A. Schulte, W. Theisen, W. Schuhmann, Visualization of local electrochemical activity and local nickel ion release on laser-welded NiTi/steel joints using combined alternating current mode and stripping mode SECM, Analyst 133 (2008) 1700.

[12] D. Ruhlig, W. Schuhmann, Spatial imaging of Cu^{2+} ion release by combining alternating current and underpotential stripping mode Scanning Electrochemical Microscopy, Electroanalysis 19 (2007) 191.

[13] D. Filotas, B. M. Fernández-Pérez, J. Izquierdo, A. Kiss, L. Nagy, G. Nagy, R. M. Souto, Improved potentiometric SECM imaging of galvanic corrosion reactions, Corrosion Science 129 (2017) 136.

[14] J. Izquierdo, A. Kiss, J. J. Santana, L. Nagy, I. Bitter, H. S. Isaacs, G. Nagy, R. M. Souto, Development of Mg^{2+} ion-selective microelectrodes for potentiometric scanning electrochemical microscopy monitoring of galvanic corrosion processes, J. Electrochem. Soc. 160 (2013) C451.

[15] P. Dauphin-Ducharme, R. M. Asmussen, D. W. Shoesmith, J. Mauzeroll, In-situ Mg^{2+} release monitored during magnesium alloy corrosion, J. Electroanal. Chem. 736 (2015) 61.

[16] S. V. Lamaka, O. V. Karavai, A. C. Bastos, M. L. Zheludkevich, M. G. S. Ferreira, Monitoring local spatial distribution of Mg^{2+}, pH and ionic currents, Electrochem. Commun. 10 (2008) 259.

[17] A. C. Bastos, M. G. Taryba, O. V. Karavai, M. L. Zheludkevich, S. V. Lamaka, M. G. S. Ferreira, Micropotentiometric mapping of local distributions of Zn^{2+} relevant to corrosion studies, Electrochem. Commun. 12 (2010) 394.

[18] K. Eckhard, X.X. Chen, F. Turcu, W. Schuhmann, Redox competition mode of scanning electrochemical microscopy (RC-SECM) for visualisation of local catalytic activity, Phys. Chem. Chem. Phys. 8 (2006) 5359.

[19] K. Eckhard and W. Schuhmann, Localised visualisation of O_2 consumption and H_2O_2 formation by means of SECM for the characterisation of fuel cell catalyst activity, Electrochim. Acta. 53 (2007) 1164.

[20] R. Leiva-García, R. Akid, D. Greenfield, J. Gittens, M. J. Muñoz-Portero, J. García-Antón, Study of the sensitisation of a highly alloyed austenitic stainless steel, Alloy 926 (UNS N08926), by means of scanning electrochemical microscopy, Electrochim. Acta 70 (2012) 105.

[21] L. C. Abodi, Y. Gonzalez-Garcia, O. Dolgikh, C. Dan, D. Deconinck, J. M. C. Mol, H. Terryn, J. Deconinck, Simulated and measured response of oxygen SECM-measurements in presence of a corrosion process, Electrochim. Acta 146 (2014) 556.

[22] J. L. Fernandez, D. A. Walsh, A. J. Bard, Thermodynamic guidelines for the design of bimetallic catalysts for oxygen electroreduction and rapid screening by scanning electrochemical microscopy. M−Co (M: Pd, Ag, Au), J. Am. Chem. Soc., 127 (2005) 357.

[23] S. S. Jamali, S. E. Moulton, D. E. Tallman, M. Forsyth, J. Weber, A. Mirabedini, G. G. Wallace, Corrosion protection afforded by praseodymium conversion film on Mg alloy AZNd in simulated biological fluid studied by scanning electrochemical microscopy, J. Electroanal. Chem. 739 (2015) 211.

[24] S. S. Jamali, S. E. Moulton, D. E. Tallman, M. Forsyth, J. Weber, G. G. Wallace, Applications of scanning electrochemical microscopy (SECM) for local characterization of AZ31 surface during corrosion in a buffered media, Corrosion Science 86 (2014) 93.

[25] A. I. Oleinick, D. Battistel, S. Daniele, I. Svir, C. Amatore, Simple and clear evidence for positive feedback limitation by bipolar behavior during scanning electrochemical microscopy of unbiased conductors, Anal. Chem. 83 (2011) 4887.

[26] R. C. Engstrom, Spatial resolution of electrode heterogeneity using iontophoresis, Anal. Chem. 56 (1984) 890.

[27] C.-L. Lin, J. Rodríguez-López, A. J. Bard, Micropipet delivery− substrate collection mode of scanning electrochemical microscopy for the imaging of electrochemical reactions and the screening of methanol oxidation electrocatalysts, Anal. Chem. 81 (2009) 8868.

[28] O. Lugaresi, J. V. Perales-Rondón, A. Minguzzi, J. Solla-Gullón, S, Rondinini, J. M. Feliu, C. M. Sánchez-Sánchez, Rapid screening of silver nanoparticles for the catalytic degradation of chlorinated pollutants in water, Appl. Catal. B 163 (2015) 554.

[29] J. V. Perales-Rondón, E. Herrero, J. Solla-Gullón, C.M. Sánchez-Sánchez, V. Vivier, Oxygen crossover effect on palladium and platinum based electrocatalysts during formic acid oxidation studied by scanning electrochemical microscopy, J. Electroanal. Chem. 793 (2017) 218.

[30] J. V. Perales-Rondón, J. Solla-Gullón, E. Herrero, C. M. Sánchez-Sánchez, Enhanced catalytic activity and stability for the electrooxidation of formic acid on lead modified shape controlled platinum nanoparticles, Appl. Catal. B 201 (2017) 48.

[31] J. V. Macpherson, N. Simjee, P. R. Unwin, Hydrodynamic ultramicroelectrodes: kinetic and analytical applications, Electrochim. Acta 47 (2001) 29.

[32] J. V. Macpherson, S. Marcar, P. R. Unwin, Microjet Electrode: A hydrodynamic ultramicroelectrode with high mass-transfer rates, Anal. Chem. 66 (1994) 2175.

[33] J. V. Macpherson, M. A. Beeston, P. R. Unwin, Imaging local mass-transfer rates within an impinging jet and studies of fast heterogeneous electron-transfer kinetics using the microjet electrode, J. Chem. Soc. Faraday Trans., 91 (1995) 899.

[34] D. A. Walsh, J. L. Fernández, J. Mauzeroll, A. J. Bard, Scanning electrochemical microscopy. 55. fabrication and characterization of micropipette Probes, Anal. Chem. 77 (2005) 5182.

[35] T. Kai, S. Chen, E. Monterroso, F. Zhou, Continuous nanoflow-scanning electrochemical microscopy: voltammetric characterization and application for accurate and reproducible Imaging of enzyme-labeled protein microarrays, Anal. Chem. 87 (2015) 4523.

[36] N. Aouina, F. Balbaud-Célérier, F. Huet, S. Joiret, H. Perrot, F. Rouillard, V. Vivier, A flow microdevice for studying the initiation and propagation of a single pit, Corrosion science 62 (2012) 1.

[37] N. Aouina, F. Balbaud-Célérier, F. Huet, S. Joiret, H. Perrot, F. Rouillard, V. Vivier, Initiation and growth of a single pit on 316L stainless steel: Influence of SO_4^{2-} and ClO_4^- anions, Electrochim. Acta 104 (2013) 274.

[38] S. Heurtault, R. Robin, F. Rouillard, V. Vivier, Initiation and propagation of a single pit on stainless steel using a local probe technique, Faraday Discuss. 180 (2015) 267.

[39] S. Heurtault, R. Robin, F. Rouillard, V. Vivier, On the propagation of open and covered pit in 316L stainless steel, Electrochim Acta. 203 (2016) 316.

[40] J.-B. Jorcin, C. Blanc, N. Pébère, B. Tribollet, V. Vivier, Galvanic coupling between pure copper and pure aluminum: experimental approach and mathematical model, J. Electrochem. Soc. 155 (2007) C46.

[41] L. Lacroix, C. Blanc, N. Pébère, G. E. Thompson, B. Tribollet, V. Vivier, Simulating the galvanic coupling between S-Al_2CuMg phase particles and the matrix of 2024 aerospace aluminium alloy, Corrosion Science 64 (2012) 213.

[42] C. Blanc, N. Pébère, B. Tribollet, V. Vivier, Galvanic coupling between copper and aluminium in a thin-layer cell, Corrosion Science 52 (2010) 991.

[43] S. M. Gateman, O. Gharbi, M. Turmine, V. Vivier, Measuring changes in wettability and surface area during micro droplet corrosion measurements, Electrochim. Acta 399 (2021) 139402.

[44] D.T. Chin, C.H. Tsang, Mass transfer to an impinging jet electrode, J. Electrochem. Soc. 125 (1978) 1461.

[45] C. G. Zoski, N. Simjee, O. Guenat, M. Koudelka-Hep, Addressable microelectrode arrays: characterization by imaging with scanning electrochemical microscopy, Anal. Chem. 76 (2004) 62.

[46] K. A. Yasakau, M. L. Zheludkevich, S. V. Lamaka, M. G. S. Ferreira, Mechanism of corrosion inhibition of AA2024 by rare-earth compounds, J. Phys. Chem. B 110 (2006) 5515.

[47] P. Visser, Y. Liu, X. Zhou, T. Hashimoto, G. E. Thompson, S. B. Lyon, L. G. J. Van der Ven, A. J. M. C. Mol, H. A. Terryn, The corrosion protection of AA2024-T3 aluminium alloy by leaching of lithium-containing salts from organic coatings, Faraday Discussions 180 (2015) 511.

[48] P. Visser, Y. Liu, H. A. Terryn, J. M. C. Mol, Lithium salts as leachable corrosion inhibitors and potential replacement for hexavalent chromium in organic coatings for the protection of aluminum alloys, J. Coat. Technol. Res. 13 (2016) 557.

[49] C. M. Sánchez-Sánchez, A. J. Bard, Hydrogen Peroxide production in the oxygen reduction reaction at different electrocatalysts as quantified by scanning electrochemical microscopy, Anal. Chem. 81 (2009) 8094.

[50] D. Filotás, B. M. Fernández-Pérez, J. Izquierdo, L. Nagy, G. Nagy, R. M. Souto, Combined amperometric/potentiometric probes for improved chemical imaging of corroding surfaces using scanning electrochemical microscopy, Electrochim. Acta 221 (2016) 48.

[51] M. C. O. Monteiro, M. T. M. Koper, Measuring local pH in electrochemistry, Curr. Opin. Electrochem. 25 (2021) 100649.